

Accelerated 2D magnetic resonance spectroscopy of single spins using matrix completion

Jochen Scheuer¹, Alexander Stark¹, Matthias Kost², Martin B. Plenio², Boris Naydenov¹, and Fedor Jelezko¹

¹Institut für Quantenoptik and Center for Integrated Quantum Science and Technology (IQST), Albert-Einstein-Allee 11, Universität Ulm, 89069 Ulm, Germany

²Institut für Theoretische Physik and Center for Integrated Quantum Science and Technology (IQST), Albert-Einstein-Allee 11, Universität Ulm, 89069 Ulm, Germany

E-mail: boris.naydenov@uni-ulm.de

Abstract. Two dimensional nuclear magnetic resonance (NMR) spectroscopy is one of the major tools for analysing the chemical structure of organic molecules and proteins. Despite its power, this technique requires long measurement times, which, particularly in the recently emerging diamond based single molecule NMR, limits its application to stable samples. Here we demonstrate a method which allows to obtain the spectrum by collecting only a small fraction of the experimental data. Our method is based on matrix completion which can recover the full spectral information from randomly sampled data points. We confirm experimentally the applicability of this technique by performing two dimensional electron spin echo envelope modulation (ESEEM) experiments on a two spin system consisting of a single nitrogen vacancy (NV) centre in diamond coupled to a single ¹³C nuclear spin. We show that the main peaks in the spectrum can be obtained with only 10 % of the total number of the data points. We believe that our results reported here can find an application in all types of two dimensional spectroscopy, as long as the measured matrices have a low rank.

Submitted to: *New J. Phys. as Fast Track Communication*

1. Introduction

A key tool in the quest for the determination of the structure of molecules and proteins is nuclear magnetic resonance spectroscopy (NMR) which has helped to make fundamental contributions to the advancement of biological sciences. This is achieved by measuring the magnetic response of molecules in a large ensemble to sequences of radio frequency pulses. This temporal response is then mapped to multi-dimensional spectra which encode the dynamical properties of the system and therefore the interactions between its constituent nuclear spins [1, 2]. The information contained in these spectra forms the basis for the determination of molecular structure. Current NMR schemes are intrinsically ensemble measurements, both due to the minute size of the nuclear magnetic moments and the tiny polarization of these nuclear spins at room temperature, even in very strong magnetic fields. Consequently, NMR can only deliver ensemble information while the structure and dynamics of individual specimens remain hidden from observation.

Recent progress in the control of the single electron spin in Nitrogen-vacancy (NV) centers in diamond offers a new perspective here, as it can make use of optically detected magnetic resonance [3, 4] for the detection of material properties [5] including minute magnetic fields [6, 7, 8, 9]. Building on this, recent theoretical investigations [10, 11, 12, 13] have suggested that NV centers implanted a few nanometers below the surface should be able to detect and locate individual nuclear spins above the diamond surface. Subsequent experimental work has indeed achieved the observation of small clusters of nuclear spins outside of diamond with a sensitivity that is sufficient to identify even individual nuclear spins [14].

One of the challenges for the determination of the structure of smaller biomolecules or even entire proteins by means of 2D spectroscopy detected by an NV center is the considerable amount of data that need to be taken which results in long measurement times. Indeed, the large amount of required data and the associated long measurement times represent a challenge that is common to both ensemble NMR and single molecule NMR measurements.

As suggested in [12] we demonstrate NV sensing experiments on nuclear spins using methods from the field of signal processing, particularly matrix completion [15, 16]. With this technique we can obtain reliably the spectral information that is contained in 2D-NMR spectra from a small subset of all accessible data points (see [17] and [18] for applications of the related but distinct compressive sensing and non-uniform sampling to bulk NMR). The results presented here show that order of magnitude reduction in the overall measurement time in NV center based 2D-NMR can be achieved.

In the remainder we briefly introduce matrix completion in Section 2. Then Section 3 presents the application of this method to concrete experimental data that have been obtained from an NV center interacting with a nearby nucleus. The results demonstrate that already a sampling rate of around 10% suffices to reconstruct the spectral information reliably. We finish with a brief conclusion and outlook concerning

the potential of this approach for diamond quantum sensing.

2. Matrix Completion Method

This section serves to introduce briefly the concept of matrix completion, the basic properties relevant to this work and the specific algorithm that we use for its application to our experimental data.

A 2D-spectrum encodes the response of a system to a sequence of pulses with varying temporal separation, denoted by t_i and τ_j , and arrange the result in a data matrix $M(i, j)$. The 2D-spectrum $S(\omega_1, \omega_2)$ is then obtained as the Fourier transform of both time coordinates in M . In our work we are sampling randomly chosen elements of the matrix M with indices (i, j) drawn from the index set Ω , leading to constraints $X_{ij} = M_{ij}$ for $(i, j) \in \Omega$. Matrix completion solves the task of obtaining the missing matrix entries of M that have not been measured in experiment. In general this is impossible unless we have further knowledge about the matrix M , namely that it typically has a low singular value rank r , i.e. $r \ll n$. Fortunately, this is indeed the case for typical data sets and especially those from 2D spectroscopy.

One possible approach to achieve this matrix completion is by solving the minimization problem

$$\min [tr|X| : |X_{ij} - M_{ij}| < \epsilon \text{ for } (i, j) \in \Omega] \quad (1)$$

where $tr|X|$ is the trace norm of the matrix X and ϵ is a given tolerance. Indeed, it can be proven that this formulation of the problem achieves the desired aim [19] as the solution of eq. (1) yields the matrix M with high probability if the number of sampled elements $|\Omega| = \mathcal{O}(nr \ln n)$ where r is the singular value rank of the $n \times n$ matrix M (see [19, 20] for proofs and a rigorous mathematical statement). This suggests that a computational gain by a factor of order $n/(r \ln n)$ may be achieved through random sampling in the manner described above (see for example [12, 21] on computed 2D-spectroscopy data).

This still leaves us with the task of solving the minimization problem eq. (1). In principle, this equation can be rewritten as a semi-definite programme and then solved employing standard solvers for convex problems. Unfortunately, standard solvers tend to be limited to relatively small matrix sizes, but fortunately alternatives exist. Indeed, [22] proposed to solve eq. (1) approximately through the so-called singular value thresholding (SVT) algorithm [22] which permits very large matrices to be treated. It is this algorithm that we will be using in our work. The SVT-algorithm solves iteratively the set of equations

$$Y^{(k-1)} = U^{(k-1)} D^{(k-1)} V^{(k-1)} \quad (2)$$

$$X^{(k)} = U^{(k-1)} \max(D^{(k-1)} - \tau \mathbb{1}) V^{(k-1)} \quad (3)$$

$$Y^{(k)} = Y^{(k-1)} + \delta_k \mathcal{P}_\Omega(M - X^{(k)}) \quad (4)$$

where $(\mathcal{P}_\Omega(M))_{ij} = M_{ij}$ for $(i, j) \in \Omega$ and zero otherwise and eq. (2) represents the singular value decomposition of the matrix $Y^{(k-1)}$. τ and δ_k are free parameters in the

procedure that regulate the soft thresholding (eq. 4) and the inclusion of the constraints (eq. 5). The choice $\delta_k < 2$ ensure provable convergence and $\tau = 5n$ for $n \times n$ -matrices represent typical values (see [22]). As a termination criterion of the iteration we employ the condition

$$\frac{\|(\mathcal{P}_\Omega(X^{(k)} - M))\|_F}{\|(\mathcal{P}_\Omega(M))\|_F} < \epsilon \quad (5)$$

for some ϵ , and $\|\cdot\|_F$ being the Frobenius norm [22]. The algorithm employs a singular value decomposition which, for large matrices, can be accelerated considerably [23, 24]. It is also noteworthy that other approaches for solving eq. (1) such as those reported in [25, 26, 27] may lead to improved performance and/or stability but for the purposes of this study SVT was sufficient and recommended itself thanks to its ease of implementation. In any real-world application, the measured entries of the data matrix will be corrupted at least by a small amount of noise. Hence the question of the robustness of the matrix completion approach to fluctuations in the experimental data arises naturally. Reassuringly, results have been developed that guarantee that reasonably accurate matrix completion is possible from noisy sampled entries [28]. In that scenario noise can be neglected if the relevant spectral information can be still extracted from the low rank approximation of M , thus implicating a sufficiently large signal-to-noise ratio and leading to the fact that noise contribution results in small singular values, which are discarded after applying our algorithm. Hence matrix completion offers three major advantages:

- Weak noise is directly suppressed by the matrix completion algorithm
- The spectrum of the system can be recovered from a small subset of all data e.g. only 10 % of the total in our examples.
- In contrast to compressed sensing, the algorithm used here does not require any additional information, e. g. the sparse basis [29].

The following section will now present the result of the application of the matrix completion algorithm to concrete experimental data that have been obtained in our laboratory.

3. Experimental Implementation

3.1. 2D ESEEM with a single NV centre

The method of matrix completion has been implemented in 2D optical spectroscopy of Rb vapour [30]. We use a single NV centre in diamond coupled to a proximal ^{13}C nuclear spin as a test system for the demonstration of the matrix completion protocol. NVs are optically active point defect centres in the diamond crystal. Their fluorescence depends on the electron spin number m_s of the triplet ground state, allowing to measure the electron spin of single centres. NVs close to the diamond surface have been used to detect few thousand external protons [31, 32] followed later by a demonstration

of even single spins sensitivity [14] leading to nano-scale magnetic resonance imaging [33, 34, 35]. For these type of experiments the data acquisition is quite long due to the low fluorescence emission from single centres.

The NV has a triplet ground state (electron spin $S = 1$) coupled to the nitrogen nuclear spin (^{14}N , $I = 1$). The system can be described by the Hamiltonian:

$$\hat{H} = D\hat{S}_z^2 + \frac{g\mu_B}{\hbar}\vec{B} \cdot \vec{S} + \vec{S} \cdot \mathbf{A}_{^{14}\text{N}} \cdot \vec{I} \quad (6)$$

where $D/2\pi = 2.87$ GHz is the zero field splitting of the ground state, $g = 2.003$ is the Landé factor, μ_B is the Bohr magneton, $\vec{B} = B_x\vec{e}_x + B_y\vec{e}_y + B_z\vec{e}_z$ is the applied static magnetic field, $\vec{S} = \hat{S}_x + \hat{S}_y + \hat{S}_z$ and $\vec{I} = \hat{I}_x + \hat{I}_y + \hat{I}_z$ are the electron and nuclear spin operators and $\mathbf{A}_{^{14}\text{N}}$ is the hyperfine interaction tensor. The z axis is taken to be along the NV crystal axis. If there is a single ^{13}C nuclear spin ($I = 1/2$) in the proximity, the following term

$$\hat{H}_{\text{HF}^{13}\text{C}} = \vec{S} \cdot \mathbf{A}_{^{13}\text{C}} \cdot \vec{I} \quad (7)$$

is added to the spin Hamiltonian (6), with $\mathbf{A}_{^{13}\text{C}}$ being the hyperfine interaction tensor to a ^{13}C nuclear spin. One of the simplest 2D NMR experiments consists of three $\pi/2$ pulses and is called correlation spectroscopy (COSY) [36]. In our work we use its "equivalent" in the electron spin resonance - the three pulse electron spin echo envelope modulation (ESEEM) pulse sequence (see [37] for more details) shown in figure 1.

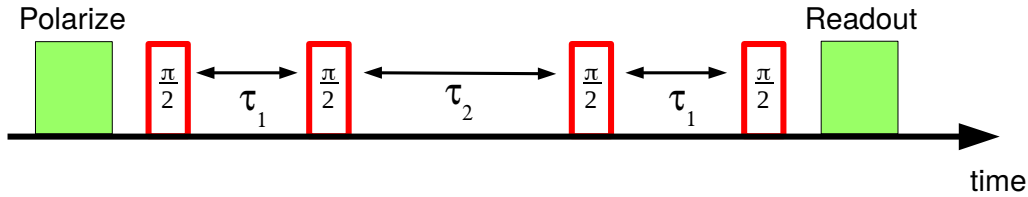


Figure 1. Pulse sequence for the two dimensional ESEEM measurement used in our experiments.

The sequence starts with a laser pulse of about $3 \mu\text{s}$ to polarize the NV electron spin in the $|m_s = 0\rangle$ state. Afterwards we apply four $\pi/2$ microwave pulses at times $t = 0$, $t = \tau_1$, $t = \tau_1 + \tau_2$ and $t = 2\tau_1 + \tau_2$. The last pulse is used to transfer the electron spin coherence into population, which is read out by the last laser pulse. The spin signal is recorded for each pair of (τ_1, τ_2) and then a 2D Fourier transform is performed giving a set of frequencies (ν_1, ν_2) . From this spectrum the number of nuclei coupled to the electron spin and the off diagonal elements of the hyperfine interaction tensor (e.g. proportional to $\hat{S}_z \hat{I}_x$) can be obtained [37].

We applied this pulse sequence in two different experiments. In the first measurement we use a single NV without resolvable coupling to ^{13}C spins. The system consists of a NV electron and a nitrogen nuclear spins, which are described by the Hamiltonian in (6). If the static magnetic field is aligned with the NV axis, the hyperfine interaction tensor $\mathbf{A}_{^{14}\text{N}}$ is diagonal and there is no ESEEM effect. In order to introduce artificial "off-diagonal" terms, we apply the static $|\vec{B}| \approx 100$ G off-axis, at an angle of about 34

degrees with respect to the z axis. The expected 2D spectrum S_{theo} can be simulated by using the Hamiltonian (6) and is plotted in figure 2a. In figure 2b we plot the Fourier

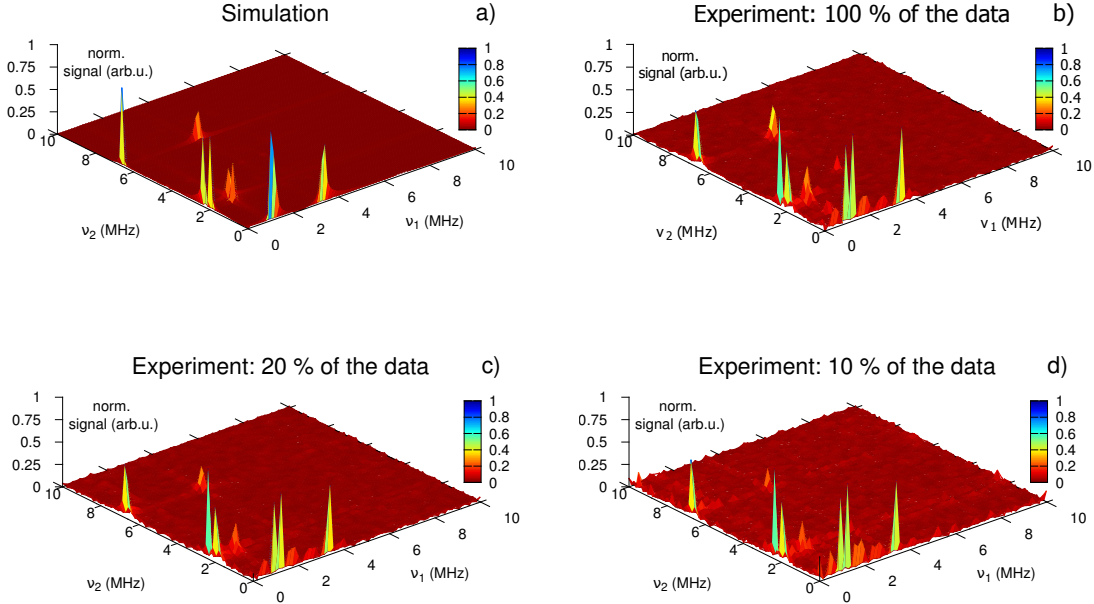


Figure 2. 2D ESEEM simulation and experimental data with a single NV when static magnetic field $B_0 = 100.9$ G is applied at an angle of 34.1° . (a) Simulation using the Hamiltonian (6). (b) Fourier transform of the complete set of the experimental data points $S_{\text{exp}}^{\text{full}}$. Fourier transform of the experimental data after applying matrix completion and using 20% $S_{\text{exp}}^{20\%}$ (c) and $S_{\text{exp}}^{10\%}$ 10% (d) of the time domain data. The main peaks are still observed even when 90% of the data is removed!

transform of the experimental data $S_{\text{exp}}^{\text{full}}$, where we use all collected data points. The experiment agrees well with the simulation. In order to demonstrate the performance of the matrix completion method, we use a random mask Ω to remove a certain part from the full experimental data in the time domain. After that, we apply matrix completion using the SVT algorithm as described in section 2 to recover the full matrix. A Fourier transform of the matrix obtained with 20% of the initial data points $S_{\text{exp}}^{20\%}$ is shown in figure 2c. Despite the removal of 80% of the recorded data, the number of peaks and their positions are still present if we compare to figure 2b. Even if we keep only 10% of the original matrix (see figure 2d), we can still recover the relevant spectral information. In the second experiment we localized an NV coupled to a single ^{13}C spin with a coupling strength of $A_{^{13}\text{C}} = 9$ MHz. Now, depending on the position of this carbon atom with respect to the NV, there are different hyperfine interaction tensors [38, 39, 40]. The spectrum can be calculated by using the Hamiltonian (6) and (7) by choosing the correct hyperfine interaction tensor. The simulation is shown in figure 3a. In these measurements the magnetic field has been aligned along the NV axis. The 2D Fourier transform of the full data set is shown in figure 3b. As in the previous experiment, we

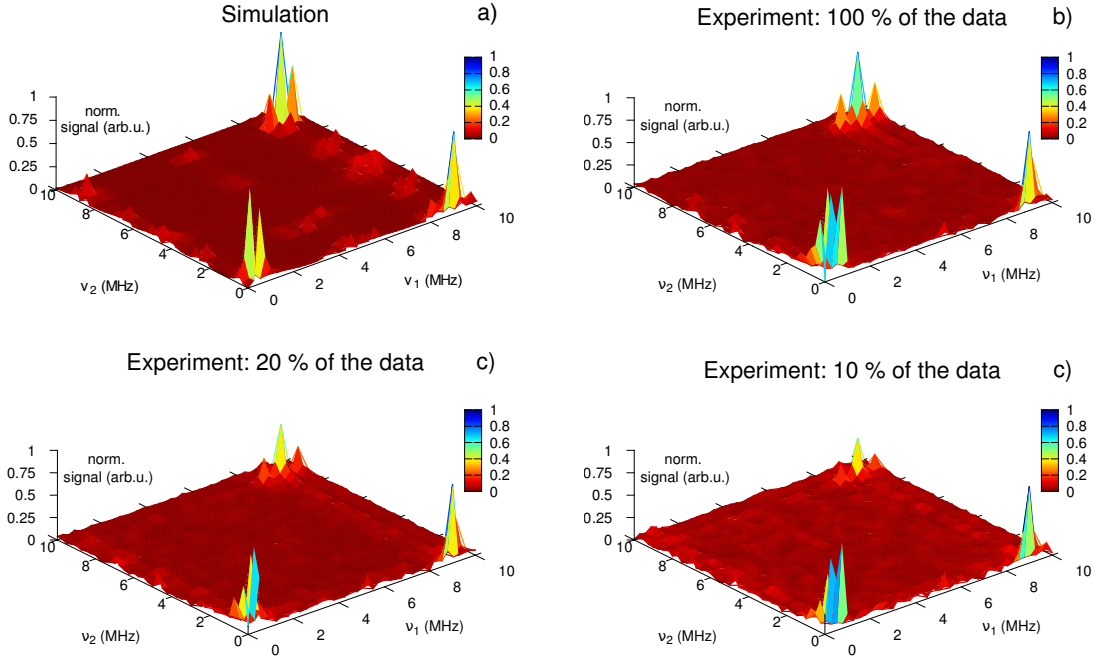


Figure 3. 2D ESEEM simulation and experimental data with a single NV coupled to a single ^{13}C nuclear spin. (a) Simulation using the spin Hamiltonian (6) and (7). (b) Fourier transform of the complete set of the experimental data points. Fourier transform of 20% (c) and 10% (d) of the data in the time domain. Here we again can recover the spectral information by keeping small amount of the experimental data.

can still recover the full spectral information (cf. figure 3c), if we remove randomly 80% of the data points. From figure 3d we can conclude that even 10% of the data suffice for the matrix completion algorithm to obtain the spectrum. In fact, this factor of ten is what is expected from the theory, see section 2 and below.

3.2. Performance of the matrix completion algorithm

In the following the performance of the matrix completion algorithm will be analysed on our experimental data. For this purpose we have to quantify how good we can recover the matrix containing the spectrum, when a small number of measurements is performed. We use the experimental data shown in figure 3. The data is stored in a matrix M_{red} with reduced number of elements different from zero. This matrix is then compared with the matrix M_{tot} , obtained by measuring the total number of points with all pairs of (τ_i, τ_j) . By using these two matrices, we define the fidelity F of our algorithm as

$$F = 1 - \frac{\|M_{\text{tot}} - M_{\text{red}}\|_F^2}{\|M_{\text{tot}}\|_F^2}. \quad (8)$$

In figure 4 we plot the fidelity as a function of the fraction of the elements of the complete matrix (red markers). In the same plot we show the ordered singular values σ_i of the matrix with the full number of points M_{tot} . From the plot we can conclude

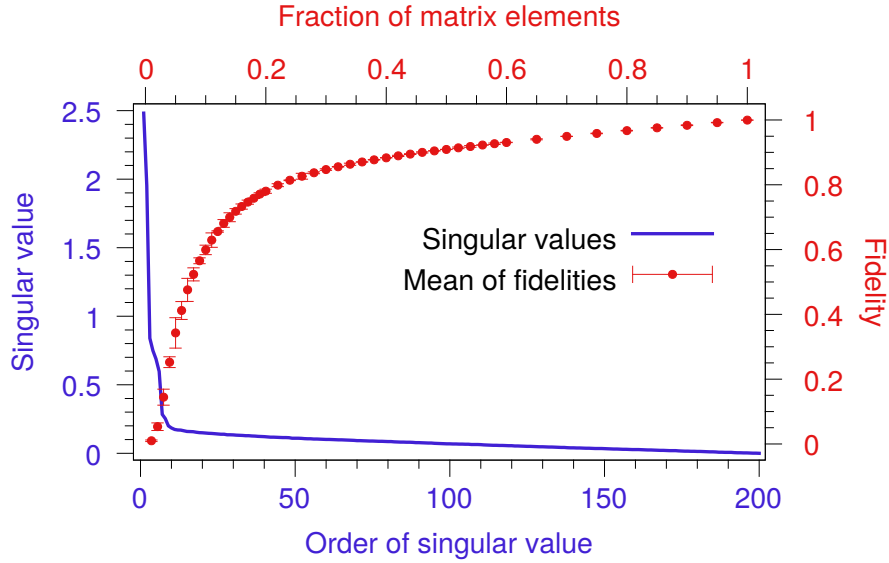


Figure 4. Mean of fidelities (red dot markers, right axis) of the matrix completion algorithm ($\tau = 100$) as a function of the fraction of sampled elements (top axis) taken from the experimental data shown in figure 3. The matrix completion algorithm was performed 128 times with each time different random sampling, here the errorbars denote the standard deviation. The blue curve (left axis) represents the singular values σ_i of the measured data (fig. 3b) in descending order.

that most of the spectral information ($> 70\%$) can be recovered by using 10% of the elements of M_{tot} , since only these elements are significantly larger than zero. This result is consistent with the theoretical limit for recovering M_{tot} given by $nr \ln n$ [19, 20] where we can roughly assume $r = 4$, which is the number of the peaks in the spectrum. The spectrum consists of few peaks, while the rest of the matrix elements contain only noise and can be discarded.

It is interesting to investigate the influence of the threshold parameter τ on the performance of the SVT algorithm and the fidelity of the so determined spectra (see Figure 5). Too small threshold values τ , e.g. at $\tau = 10$ or $\tau = 20$ (pink and orange markers), lead to low fidelity when less than 60% of the matrix elements are sampled. We can achieve higher fidelities F by increasing τ and we observe saturation around $\tau = 100$. That is, for $\tau \gg 100$ we cannot obtain higher significantly higher fidelities, while the required computation time (equivalent to the number of iterations) increases which can be seen in the inset graph in figure 5. From there we can conclude that with our data set thresholds even below the empirically suggested rule $\tau = 5n \approx 1000$ for our case of $n = 201$ (see section 2 and [22]) are sufficient. A python script can be found in the supplementary information, where the SVT algorithm is implemented, together with the data set from figure 3b.

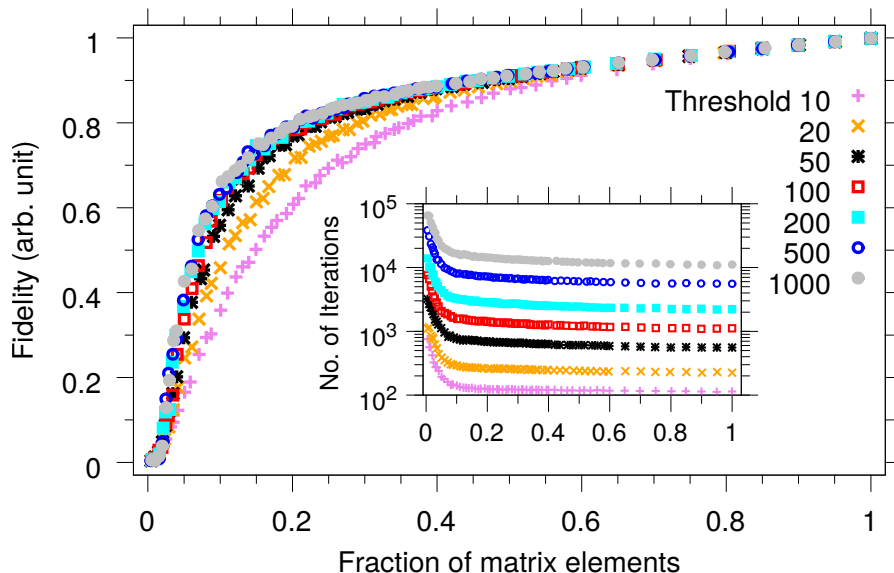


Figure 5. The fidelity of the matrix completion algorithm as a function of the fraction of the matrix elements at different thresholds τ . Inset: Number of iterations required to run the matrix completion algorithm as a function of the threshold and the fraction of the matrix elements. The performance calculation are based on data shown in figure 3.

4. Conclusions

In summary, we have demonstrated the application of a method for reconstructing a two dimensional ESEEM spectrum, by collecting only small part of the data in the time domain. With our technique we can obtain the necessary spectral information by measuring 10% of the experimental data points in two different experiments. By using our method, the measurement time can be shortened by a factor 10 at the same signal-to-noise ratio compared to the conventional experiment. We believe that the reported results will be useful for any type 2D NMR and ESR spectroscopy and also for magnetic resonance imaging. Our method is particularly useful for single spins experiments, which usually require very long measurement times [35, 13].

Acknowledgement

This work has been supported by DFG (SFB TR21, FOR 1493), Alexander von Humboldt Foundation, Volkswagenstiftung and EU (STREP Project DIADEMS, EQuaM, SIQS, ERC Synergy Grant BioQ). BN is grateful to the Bundesministerium für Bildung und Forschung (BMBF) for the ARCHES award.

References

- [1] J. Jeener. reprinted in *NMR and More in Honour of Anatole Abragam*, Eds. M. Goldman and M. Porneuf. In *Lecture Notes of the Ampere School in Basko Polje, Yugoslavia 1971*, pages 1–379, 1994.
- [2] R.R. Ernst, G. Bodenhausen, and A. Wokaun. *Principles of Nuclear Magnetic Resonance in One and Two Dimensions*. Oxford University Press, Oxford, 1989.
- [3] J. Köhler, J.A.J.M. Disselhorst, M.C.J.M. Donckers, E.J.J. Groenen, J. Schmidt, and W.E. Moerner. *Nature*, 363:242, 1993.
- [4] J. Wrachtrup, C. von Borczykowski, J. Bernard, M. Orrit, and R. Brown. *Nature*, 363:244, 1993.
- [5] A. Gruber, A. Dräbenstedt, C. Tietz, L. Fleury, J. Wrachtrup, and C. von Borczykowski. *Science*, 276:2012, 1997.
- [6] B.M. Chernobrod and G.P. Berman. *J. Appl. Phys.*, 97:014903, 2005.
- [7] C. L. Degen. *Appl. Phys. Lett.*, 92:243111, 2008.
- [8] J. R. Maze, P. L. Stanwix, J. S. Hodges, S. Hong, J. M. Taylor, P. Cappellaro, L. Jiang, M. V. Gurudev Dutt, E. Togan, A. S. Zibrov, A. Yacoby, R. L. Walsworth, and M. D. Lukin. *Nature*, 455:644.
- [9] G. Balasubramanian, I. Y. Chan, R. Kolesov, M. Al-Hmoud, J. Tisler, C. Shin, C. Kim, A. Wojcik, P. R. Hemmer, A. Krueger, T. Hanke, A. Leitenstorfer, R. Bratschitsch, F. Jelezko, and J. Wrachtrup. *Nature*, 455:648, 2008.
- [10] J.-M. Cai, F. Jelezko, M. B. Plenio, and A. Retzker. *New J. Phys.*, 15:013020, 2013.
- [11] V. S. Perunicic, L. T. Hall, D. A. Simpson, C. D. Hill, and L. C. L. Hollenberg. *Phys. Rev. B*, 89:054432, 2014.
- [12] M. Kost, J.-M. Cai, and M.B. Plenio. <http://arxiv.org/abs/1407.6262>, 2014.
- [13] A. Ajoy, U. Bissbort, M.D. Lukin, R. L. Walsworth, and P. Cappellaro. *Phys. Rev. X*, 5:011001, 2015.
- [14] C. Müller, X. Kong, J.-M. Cai, K. Melentijevic, A. Stacey, M. Markham, D. Twitchen, J. Isoya, S. Pezzagna, J. Meijer, J.F. Du, M.B. Plenio, B. Naydenov, L.P. McGuinness, and F. Jelezko. *Nat. Commun.*, 5:4703, 2014.
- [15] E.J. Candes and M. B. Wakin. *IEEE Signal Process. Mag.*, 25:21, 2008.
- [16] J.-F. Cai, E. J. Candes, and Z. Shen. *SIAM J. on Optimization*, 20:1956, 2010.
- [17] D.J. Holland, M.J. Bostock, L.F. Gladden, and D. Nietlispach. *Angew. Chem. Int. Ed.*, 50:6548, 2011.
- [18] M. Mobli and J. C. Hoch. *Prog. Nucl. Magn. Reson. Spectrosc.*, 83:21, 2014.
- [19] E. J. Candès and B. Recht. *Foundations of Computational Mathematics*, 9:717, 2009.
- [20] D. Gross. *IEEE Trans. Inf. Theory*, 57:1548, 2011.
- [21] J. Almeida, J. Prior, and M.P. Plenio. *Journal of Physical Chemistry Letters*, 3:2692, 2012.
- [22] J.-F. Cai, E. J. Candès, and Z. Shen. *SIAM J. on Optimization*, 20:1956, 2008.
- [23] N. Halko, P. Martinsson, and J. Tropp. *SIAM Review*, 53:217, 2011.
- [24] D. Tamascelli, R. Rosenbach, and M.B. Plenio. <http://arxiv.org/abs/1504.00992>, 2015.
- [25] R.H. Keshavan, A. Montanari, and S. Oh. *IEEE Trans. Inf. Theory*, 56:2980, 2010.
- [26] W. Dai and O. Milenkovic. *IEEE Trans. Signal Process.*, 59:3120, 2011.
- [27] L. Balzano, R. Nowak, and B. Recht. <http://arxiv.org/abs/1006.4046>, 2010.
- [28] E. J. Candes and Y. Plan. *Proc. IEEE*, 98:925, 2010.
- [29] D. Ma, V. Gulani, N. Seiberlich, K. Liu, J. L. Sunshine, J. L. Duerk, and M. A. Griswold. *Nature*, 495:187, 2013.
- [30] J. N. Sanders, S. K. Saikin, S. Mostame, X. Andrade, J. R. Widom, A. H. Marcus, and A. Aspuru-Guzik. *J. Phys. Chem. Lett.*, 3:2697, 2012.
- [31] T. Staudacher, F. Shi, S. Pezzagna, J. Meijer, J. Du, C. A. Meriles, F. Reinhard, and J. Wrachtrup. *Science*, 339:561, 2013.
- [32] H. J. Mamin, M. Kim, M. H. Sherwood, C. T. Rettner, K. Ohno, D. D. Awschalom, and D. Rugar.

- Science*, 339:557, 2013.
- [33] D. Rugar, H. J. Mamin, M. H. Sherwood, M. Kim, C. T. Rettner, K. Ohno, and D. D. Awschalom. *Nature Nanotech.*, 10:120, 2015.
- [34] T. Häberle, D. Schmid-Lorch, F. Reinhard, and J. Wrachtrup. *Nature Nanotech.*, 10:125, 2015.
- [35] S. J. DeVience, L. M. Pham, I. Lovchinsky, A. O. Sushkov, N. Bar-Gill, C. Belthangady, F. Casola, M. Corbett, H. Zhang, M. Lukin, H. Park, A. Yacoby, and R. L. Walsworth. *Nature Nanotech.*, 10:129, 2015.
- [36] C. Slichter. *Principles of Magnetic Resonance*. Springer-Verlag, 1996.
- [37] A. Schweiger and G. Jeschke. *Principles of pulse electron paramagnetic resonance*. Oxford University Press, 2001.
- [38] A. P. Nizovtsev, S. Ya. Kilin, V. A. Pushkarchuk, A. L. Pushkarchuk, and S. A. Kuten. *Optics and Spectroscopy*, 108:230, 2010.
- [39] A. P. Nizovtsev, S. Ya. Kilin, P. Neumann, F. Jelezko, and J. Wrachtrup. *Optics and Spectroscopy*, 108:239, 2010.
- [40] A. P. Nizovtsev, S. Ya. Kilin, A. L. Pushkarchuk, V. A. Pushkarchuk, and F. Jelezko. *New J. Phys.*, 16:083014, 2014.